Sustainable Cities and Society 47 (2019) 101487

Contents lists available at ScienceDirect

Sustainable Cities and Society

journal homepage: www.elsevier.com/locate/scs

Local climate zone ventilation and urban land surface temperatures: Towards a performance-based and wind-sensitive planning proposal in megacities

Jun Yang[a,b,*], Shanhe Jin[a,b], Xiangming Xiao[c,d], Cui Jin[a], Jianhong (Cecilia) Xia[e], Xueming Li[a], Shijun Wang[f]

[a] Human Settlements Research Center, Liaoning Normal University, 116029, Dalian, China
[b] Jangho Architecture College, Northeastern University, Shenyang, 110169, China
[c] Department of Microbiology and Plant Biology, Center for Spatial Analysis, University of Oklahoma, Norman, OK, 73019, USA
[d] Ministry of Education Key Laboratory of Biodiversity Science and Ecological Engineering, Institute of Biodiversity Science, Fudan University, Shanghai, 200433, China
[e] School of Earth and Planetary Sciences, Curtin University, Australia
[f] School of Geographical Sciences, Northeast Normal University, Changchun, Jilin Province, China

ARTICLE INFO

Keywords:
Performance-based planning
Urban heat island
Local climate zone
Frontal area density
Land surface temperature

ABSTRACT

Performance-based planning (PBP) is designed to determine city planning standards based on local activity characteristics; however, there have been few practical applications of this method. This study applied PBP to assess the impact of urban building morphology on local climate surface temperatures under different wind conditions during 2017 in Shanghai, China using multi-source data, such as frontal area density (FAD), local climatic zone classification, land surface temperature (LST) data, and geographic information. The results showed that urban architectural patterns were one of the important drivers of climate change. High-density high-rise buildings can increase surface temperatures, which were evidenced in Local Climate Zone 4 (LCZ4), LCZ7, and LCZ8 in the city center. A correlation between building FAD and local climate surface temperature was 0.44 during the winter. Also, we found that although seasonal differences affected by wind direction were small, the same wind had different effects on the surface of urban buildings in different climate zones. These findings provide a reference for urban architecture planning and can help to develop urban heat island adaptation strategies based on local conditions.

1. Introduction

Urban climatology is a rapidly growing field, as urban climatic change poses a threat to the built environment, urban landscapes and urban tourism (Liu, Cheng, Jiang, & Huang, 2019; Santamouris, Cartalis & Synnefa, 2015). As part of the ecosystem, good urban planning is a guarantee of sustainable urban development (Bai, 2018). Performance-based planning (PBP) changes the traditional zoning approach to ensure flexibility of land use localization (Frew, Baker, & Donehue, 2016). Over the past 30 years, China's urbanization has developed rapidly, and land use change has altered regional ecological services and ecological environment (Liu, Wang, Wang, Wang, & Deng, 2018; Long, Liu, Hou, Li, & Li, 2014). In addition, massive emissions of carbon dioxide have caused the greenhouse effect, and haze pollution has promoted the urban heat island effect, which affects residents' quality of life (Cao et al., 2016). The spatial distribution of land cover has a certain impact on surface temperatures (Chen & Zhang, 2017). The surface temperatures of urban construction coverage are high, and those of vegetation coverage are low (Zhou, Huang, & Cadenasso, 2011). Indeed, high vegetation cover in residential areas has a cooling effect (Rotem-Mindali, Michael, Helman, & Lensky, 2015). Anthropogenic heat emissions are also dependent on architectural spatial patterns (Zhou, Weng, Gurney, Shuai, & Hu, 2012). In addition, natural ventilation strips affect changes in local urban climate (Xu et al., 2017).

Traditional planning used a community-based approach to regional analysis, while using a performance-based approach to planning land provides landowners with a high degree of flexibility (Ottensmann, 2005). O'Harrow pointed out that the use of a performance-based approach as a means of industrial planning (O'Harrow, 1958). Furthermore, standardizing urban architecture through quantitative

* Corresponding author at: Human Settlements Research Center, Liaoning Normal University, 116029, Dalian, China.
E-mail addresses: yangjun@lnnu.edu.cn (J. Yang), 359296196@qq.com (S. Jin), xiangming.xiao@ou.edu (X. Xiao), cuijin@lnnu.edu.cn (C. Jin), c.xia@curtin.edu.au (J.C. Xia), lixueming999@163.com (X. Li), wangsj@nenu.edu.cn (S. Wang).

https://doi.org/10.1016/j.scs.2019.101487
Received 26 November 2018; Received in revised form 21 February 2019; Accepted 21 February 2019
Available online 22 February 2019
2210-6707/ © 2019 Elsevier Ltd. All rights reserved.

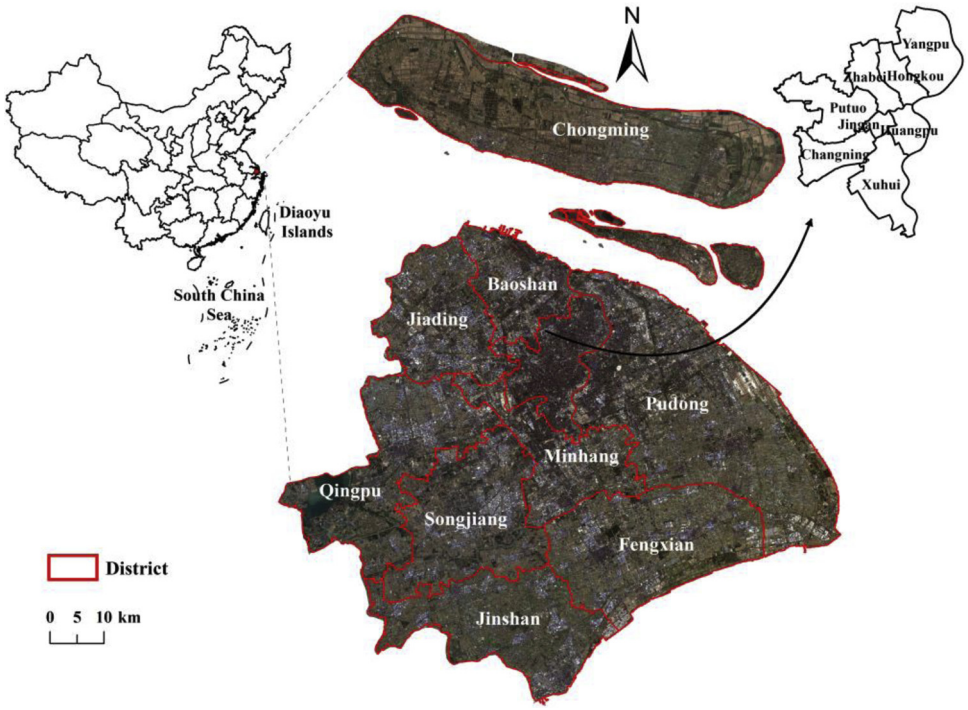

Fig. 1. Location of the study area (Shanghai, China).

performance standards is possible (Marwedel & Marwedel, 1998). A performance-based approach can assess the urban environment and development based on local characteristics. In megacities, which have relatively high and low temperatures, it is extremely important to conduct local climate classification studies. Local climate zone classification uses a combination of four different indices: urban structure, surface cover, urban texture, and anthropogenic heat sources (Oke, Mills, Christen, & Voogt, 2017; Stewart & Oke, 2012). Based on grid data, Geographical Information Systems (GIS) have been used to define and classify local climate zones in the high-density city of Hong Kong (Zheng et al., 2017). Remote sensing of surface temperatures has also been widely applied to study urban thermal environments (Dwivedi & Khire, 2018; Qiao, Tian, & Xiao, 2013; Voogt & Oke, 2003). In particular, Landsat 8 data are used to calculate hotspot temperatures based on pixels (Bokaie, Zarkesh, Arasteh, & Hosseini, 2016). Moreover, land-use regression models can provide a precise assessment of urban heat island effects, and have indicated that the impact of building architecture in complex; for example, high-density urban environments, can significantly change microclimate conditions by disrupting the wind (Shi, Katzschner, & Ng, 2017). China's urbanization development is still in progress, and overall planning of building space distribution is beneficial to urban development (Yue, Liu, & Fan, 2013). Other studies have used experimental and actual data to analyze temporal and spatial changes in urban heat islands, suggesting that wind speed, clouds, and fog are major variables that cause variations in urban climate (Bernard, Musy, Calmet, Bocher, & Keravec, 2017). The wind environments around buildings are different in summer and winter (He, Yang, & Ye, 2014).

The urban wind environment is therefore an important factor impacting urban microclimates. At present, research on urban wind environments can be categorized into studies on high-altitude urban canopies and urban near-ground wind fields. Sea breezes in coastal cities change the urban boundary layer wind field and reduce the urban heat island (Ribeiro et al., 2018). Urban expansion inevitably changes the characteristics of wind circulation (Shen, Sun, & Yuan, 2018). In residential complexes, a staggered arrangement of buildings seems to be more conducive to eliminating the wind effect of the roadway than is an alignment arrangement (Chang et al., 2016). There is a certain wind pressure around high-rise buildings (Meng et al., 2018). In addition to wind speed, direction, and frequency, the frontal area density (FAD) of urban buildings defines the urban wind environment (Ng, Yuan, Chen, Ren, & Fung, 2011). In the late 1990s, building grids were used for the first time to calculate the frontal area index (Bottema & Mestayer, 1998). The frontal area index describes the average value of urban forms at the level of the entire urban canopy. The interaction between urban buildings changes the structure of the near-surface wind environment, the obstruction of which (e.g., by high-rise buildings) can have a significant effect on the urban climate (Abd Razak, Hagishima, Ikegaya, & Tanimoto, 2013; Qiao et al., 2017). Similarly, urban ventilation and improved urban climate have been achieved by considering the frontal area index of buildings on the Kowloon Peninsula, Hong Kong (Wong & Nichol, 2013). However, urban ventilation simulation calculations have generally focused on the Hong Kong region; research on mainland areas of China is still lacking.

To achieve sustainable urban development, studies have shown that performance-based approaches can be used to better understand local land use in order to regulate and utilize land (Baker, Sipe, & Gleeson, 2006). Optimizing the urban form can mitigate the impact of future urban heat islands (Yin, Yuan, Lu, Huang, & Liu, 2018). In addition, green spaces provide important cooling benefits (Yang, Sun, Ge, & Li, 2017). Green school projects have been launched in some areas of China to significantly promote sustainable development (Zhao, He, & Meng, 2015). Furthermore, potential ventilation paths can be planned (Hsieh & Huang, 2016), and enable cool, fresh air to infiltrate cities and reduce urban air pollution and heat island effects.

Most urban planning takes into account land use, urban building performance, and urban ecological environment. Studies considering local effects of urban ventilation on urban climate are sparse. To address this gap in knowledge, considering the link between urban ventilation and land surface temperature, in order to improve the wind environment and alleviate various negative environmental problems in urban areas, this study combines the PBP method to analyze the impact of wind environment on urban surface temperature in local climate zones in Shanghai and examined the correlations between different

Table 1
Data sources and descriptions.

	Data		
	Landsat8 OLI/TIRS	Building data	Meteorological data
Resolution	15 m(Panchromatic) 30 m(Multi-Spectral) 100 m(Thermal)	Building structure outline, height, the number of floors (stories)	Temperature, Wind speed, Wind direction.
Time	2017-02-13 T 02:25:21 2017-04-02 T 02:24:34 2017-08-24 T 02:25:29 2017-10-27 T 02:25:42	2017	2017
Data sources	USGS	Baidu Map	https://rp5.ru/

urban local climate zones' FAD and surface temperatures. Data were derived from multiple sources, including building architecture and remote sensing, in conjunction with GIS methods, urban local climate zone data, and surface temperature inversion methods.

2. Data and methods

Shanghai is located at 120°52′–122°12′ E and 30°40′–31°53′ N, on the east coast of China, and covers an area of 6340 km^2 (Fig. 1). Its location represents the boundary between China's northern and southern coasts and is the site of the confluence and estuary of the Yangtze and Huangpu rivers. Shanghai's climate is influenced by subtropical monsoons, with four distinctive seasons and abundant sunshine and rainfall. The climate is mild and humid, with shorter spring and fall seasons and longer summer and winter seasons.

The original data used in this study were Landsat 8 OLT/ Thermal Infrared Sensor (TIRS) data (Table 1), data on Shanghai's municipal architecture (Fig. 2), and classified Shanghai land-use data using remote sensing images. Buildings were categorized according to the current national 'Code for Design of Civil Buildings' (GB50352-2005; (China MOCP, 2005), along with development in Shanghai (Table 2).

2.1. Local urban climate division

The construction environment seriously affects urban environmental quality (Liu, Yue, Fan, Zhang, & Huang, 2017). The spatial layout of the urban form can produce local microclimates with significant impacts on temperature (Bai et al., 2017). This study on local urban climate was conducted based on local urban climate distinctions or zones (Oke, 2006). Individual local climate zones are defined mainly by buildings and land cover (Stewart, Oke, & Krayenhoff, 2014). According to the development of Chinese cities, there are a large number of buildings with about 30 floors in the city, with the heights of the main buildings being significantly different (Zhang & Gu, 2013). Therefore, the urban building climate zones can be divided into 10 standard types (Table 3). Based on Landsat 8 remote sensing data and classified land-use types (Zhou, Zhao, Liu, Zhang, & Zhu, 2014; Zhou, Cadenasso, Schwarz, & Pickett, 2014; Zhu, Woodcock, Rogan, & Kellndorfer, 2012), the remote sensing image was iterated 20 times by unsupervised classification, and the same land use type was merged by manual interpretation; eight land use types were identified. This study statistically calculated the proportions of different land-use types within each grid. Land cover indicates the land type within the local climate zone classification grid, and buildings were classified based on height and density indices (Nassar, Blackburn, & Whyatt, 2016). A local climate zone classification map was generated by spatially merging land-use and building types.

2.2. Frontal area density

Shanghai is a rapidly growing city, with high and densely spaced buildings in the central area. Buildings with this urban pattern inevitably affect the wind field. The study area was divided using regular grids, according to the footprints of buildings; the required accuracy

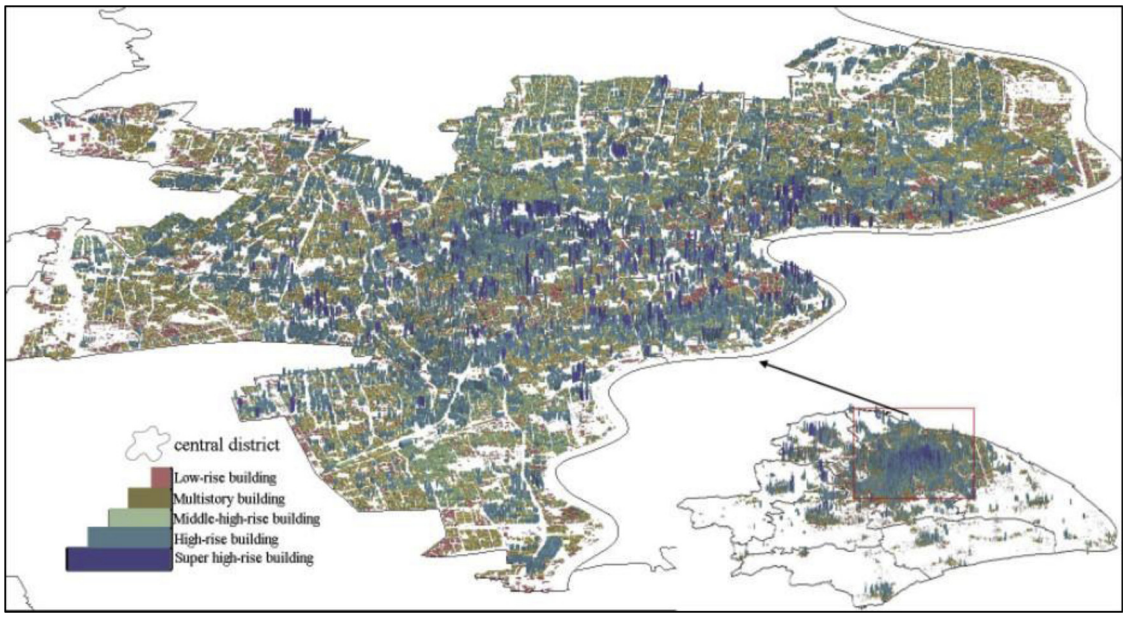

Fig. 2. Three-dimensional display of building data (height *8) for Shanghai, China.

Table 2
Building height classification.

Building type	Classification standard/floor	Introduction
Low-rise building	1–3	Brick and concrete structure
Multistory building	4–6	Brick and concrete structure
Middle-high rise building	7–9	Reinforced concrete structure
High-rise building	10–39	Reinforced concrete or glass
Super high-rise building	> = 40	Reinforced concrete or glass

Table 3
Local climate zone (LCZ) building classification system.

LCZ types	Building LCZ
LCZ 1	High-density super high building
LCZ 2	High-density high-rise building
LCZ 3	High-density middle-high rise building
LCZ 4	High-density multi-story building
LCZ 5	High-density low-rise building
LCZ 6	Low-density super high building
LCZ 7	Low-density high-rise building
LCZ 8	Low-density middle-high rise building
LCZ 9	Low-density multi-story building
LCZ 10	Low-density low-rise building

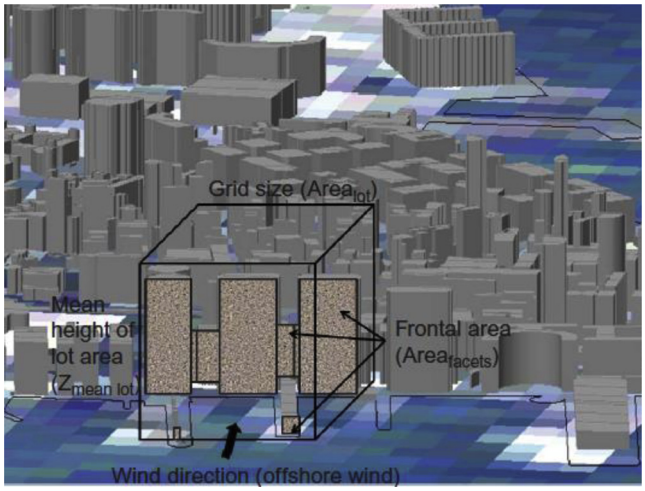

Fig. 3. Urban surfaces for the calculation of the frontal area index (Wong & Nichol, 2013).

was a 30-m grid size (Peng, Wong, Nichol, & Chan, 2016; Fig. 3):

$$\lambda f(Z,\theta) = \frac{A(\theta)proj(Z)}{AT} \quad (1)$$

where $\lambda_{f(Z,\theta)}$ is the frontal area density; $A(\theta)$ is the wind direction close to the specified height increment z; and A_T is the total area of the study area, namely the grid area.

The wind environment surrounding a single building is affected by multiple factors, such as building orientation and length, adjacent buildings, and wind direction. The windward side area of a building varies depending on the actual wind direction, and, similarly, air circulation varies depending on the urban spatial grid. The FAD focuses on changes in urban building forms at a specific height increment in a selected research area (Yuan, Ren, & Ng, 2014) and can be expressed as follows:

$$\lambda f(Z) = \sum_{i=1}^{16} \lambda f(Z,\theta) \times P\theta,i \quad (2)$$

where $\lambda_{f(z)}$ represents the frontal area density for a specific wind direction, and Pθ,i represents the frequency of a specific wind direction. This study used 16 as the value for the wind direction.

The increment of building heights must be obtained to acquire the parameters of FAD. Building heights were calculated using statistical analysis with GIS. As shown in Fig. 2, most buildings in the study area were low multi-story buildings along with some ultra-high buildings. The selected height range was 3–228 m. Using programming to complete single wind direction FAD calculations, we calculated the area of the windward surface of the building and the grid area ratio in the grid, and finally obtained the FAD of the area according to the wind frequency weighted FAD in different directions.

2.3. Surface temperature inversion

In this study, the single-window algorithm was used to calculate the surface temperature (Qin, Zhang, & Karnieli Berliner, 2001). The proposed single-window algorithm was only applicable to TM6 data with one thermal infrared band. Since the accuracy of the surface temperature inversion calculated by the single-window algorithm was higher than that using the radiation conduction formula, this study combined the single-window algorithm with the TM10 band of Landsat 8 to perform the inversion of the surface temperature. Atmospheric parameters were used to estimate the surface temperature:

$$T_s = \frac{(a(1\text{-}C\text{-}D) + (b(1\text{-}C\text{-}D)+C+D)T_{10} - DT_a)}{C\text{-}273.15}$$
$$C = \varepsilon\tau$$
$$D = (1\text{-}\tau)(1+(1\text{-}\varepsilon)\tau) \quad (3)$$

where T_s is the surface temperature (K), and a and b are coefficients fitted according to the relationship between the intensity of heat radiation and the brightness and temperature. When brightness or temperature range from 10 °C to 40 °C, the value of a is —67.355351, and the value of b is 0.458660. The T_{10} is the brightness of the sensor, T_a is the average atmosphere applied temperature (K), ε is the surface emissivity, and τ is the atmospheric transmittance of T_{10}.

3. Results

3.1. Local climate differentiation

According to the method for urban local climate division, a 30 × 30 m grid was applied, and the study area was divided into 1,019,697 cells. The height and density of buildings in grids were statistically counted and merged with the land cover data to obtain a map of urban local climate zones.

As shown in Fig. 4, the lowest urban buildings were 3 m and the highest were 228 m high. According to the overall spatial distribution (Fig. 5), most of the buildings on both sides of the Yangtze River were high-density buildings, especially east of the river; the local climate zones here were LCZ3 and LCZ4; the rural–urban fringe, such as the Jiading, Qingpu, and Songjiang districts, mostly comprised local climate types LCZ8 and LCZ9. In the central urban area, the spatial distribution of buildings tended to be aggregative; most of the buildings here were middle- and high-rise buildings, whereas most buildings in the Baoshan District, an industrial park, were low-rise and multi-story. The urban building density in urban center areas was the highest, as the building density in grids in these areas reached 100%. The urban local

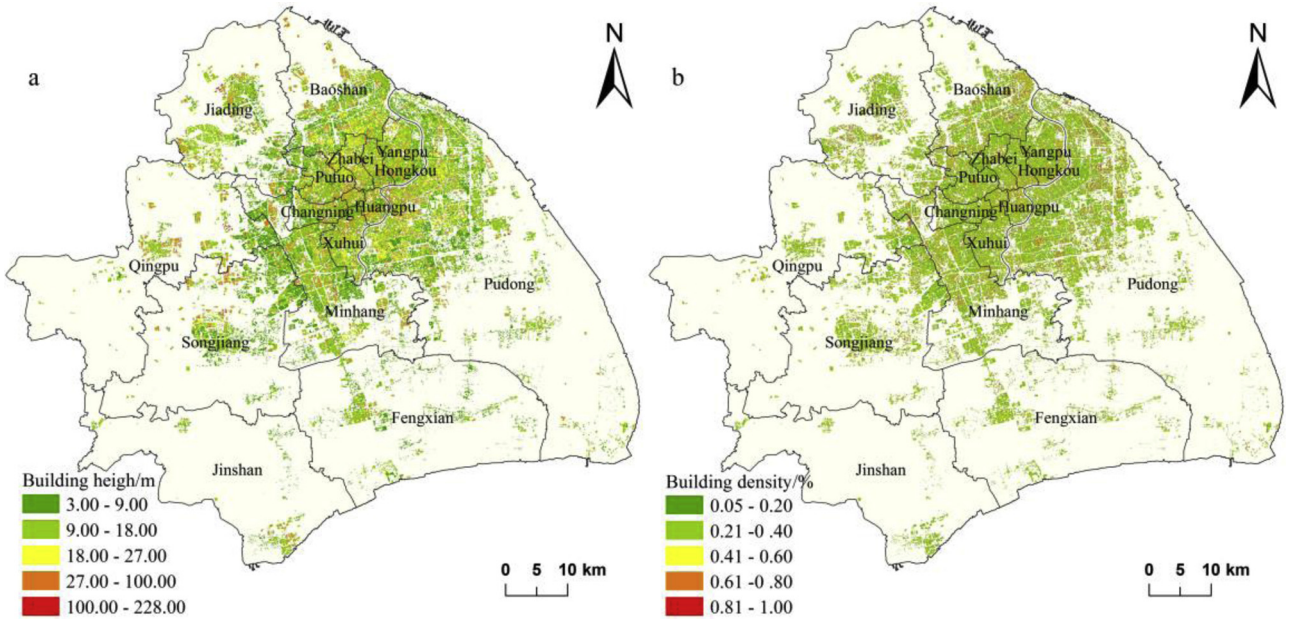

Fig. 4. Building space distribution of Shanghai in terms of building height (a) and building density (b).

climate zones were distinguished based on building height and density index. In terms of local climate zones, the major building types were high-density multi-story buildings, high-density low-rise buildings, low-density multi-story buildings, and low-density low-rise buildings, which accounted for 1.8%, 1.4%, 0.7%, and 0.5%, respectively.

3.2. Building windward differentiation

Wind speed and 16 wind directions were monitored over the four seasonal quarters of 2017 and statistically analyzed (Fig. 6). The wind speed was steady throughout the year. The major wind directions were easterly in the spring, summer, and winter, and southerly in the fall. The wind frequency was weighted, and GIS methods were used to calculate the frontal area density (Fig. 7), which indicates the ventilation strength. The larger the frontal area density, the stronger the capacity to slow the wind speed, and vice versa. According to our calculations, the urban frontal area density for the winter, spring, summer, and fall of 2017 were 0.05–16.25, 0.11–17.38, 0.11–17.09, and 0.10–16.17, respectively. These values were related to building form. All windward-side densities demonstrated spatial distribution characteristics that gradually decreased moving outward from the urban center.

The urban central areas of Shanghai include the Yangpu, Hongkou, Zhabei, Putuo, Changning, Xuhui, Huangpu, and Jingan districts.

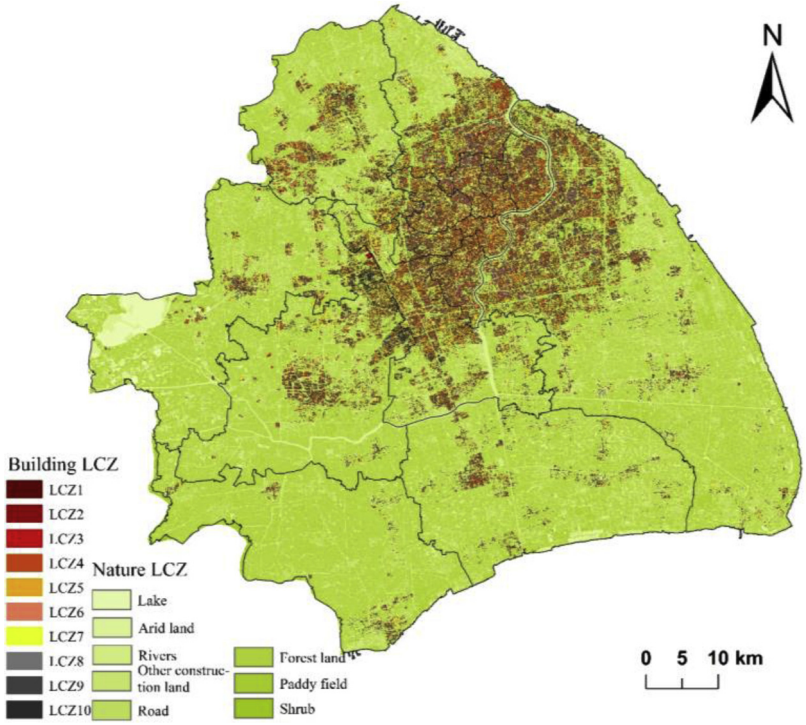

Fig. 5. Urban local climate zone (LCZ) map of Shanghai.

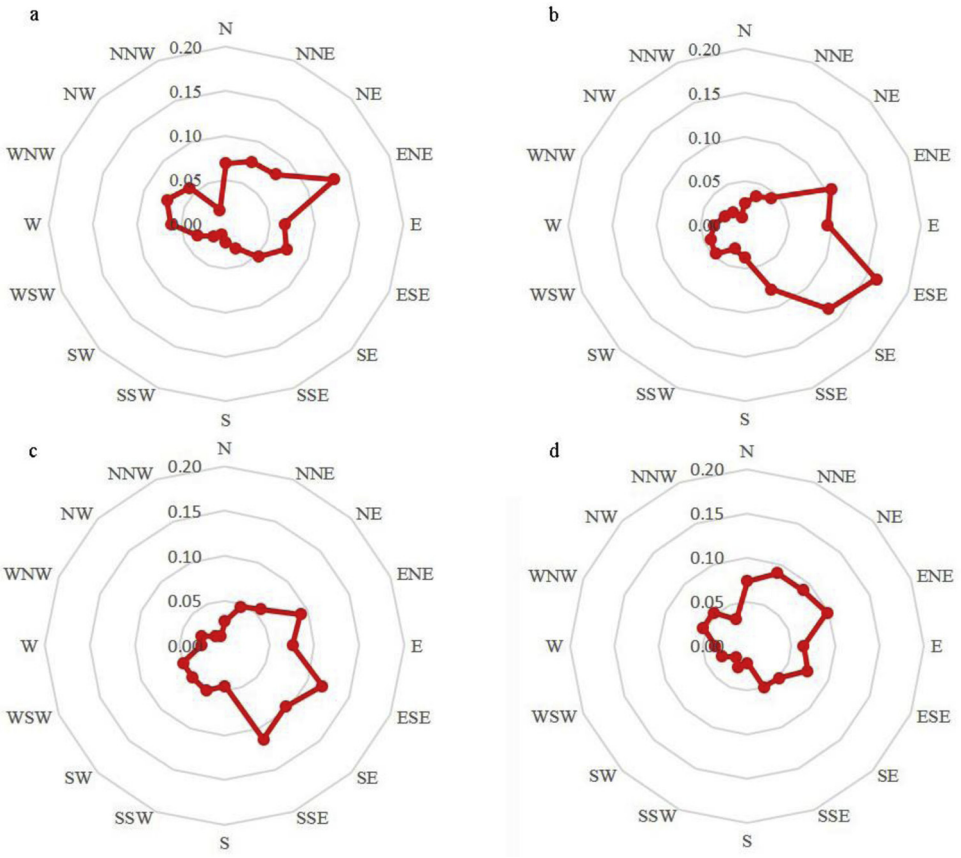

Fig. 6. Wind direction and frequency in Shanghai in the winter (a), spring (b), summer (c), and fall (d).

Owing to high-rise buildings and their dense spacing in the urban center, the atmospheric conditions over the tops of the buildings may not reach down into the deep street valleys that contribute to the wind environment at the pedestrian level, especially in the Putuo and Jingan districts. In the former, the windward-side densities for the year mainly ranged from 0.4 to 0.8, and those in the latter mainly ranged from 0.3 to 1.5 (Table 4). The results also show that building and FAD values in the Baoshan District, an industrial park near the waterfront, are high.

3.3. Surface temperature differentiation

The temperature is most affected by the surface morphology of the underlying city. The local climate can be estimated through inversion of the urban surface temperature. Shanghai's climate is characterized as subtropical and monsoon-influenced. This study selected remote sensing data and conducted inversion of the urban surface temperature for each season.

Figs. 8 and 5 show that the surface temperature distribution was closely related to the distribution of buildings. LST in the study area during different seasons showed the highest surface temperatures in the building coverage area and lower temperatures in the vegetation coverage area. In winter, spring, summer, and fall, the average temperatures were 15 °C, 23 °C, 30 °C, and 23 °C, respectively. In winter, the temperature is 15 °C – 17 °C for 45% of the time; the highest temperature in summer is 41 °C, indicating extreme high temperature; the spring LST is 23 °C – 25 °C for 36% of the time; the fall LST is 21 °C – 23 °C for 36% of the time. There were more green spaces in areas with low building heights and densities. In these areas, the building frontal area density was lower, ventilation efficiency was higher, and the temperature was relatively lower. In contrast, in areas with high urban building densities and heights, buildings covered larger areas, suggesting that the ventilation efficiency was lower and the temperatures higher.

3.4. Relationship between building FAD and local climate

Pearson's correlation analysis was used according to the classification of local climate zones to analyze the interaction between the frontal area density of different buildings and local climate.

As shown in Fig. 9, the surface temperature is related to the urban FAD in the local climate zone. Different local climate zone types have different effects on urban ventilation and surface temperature. Overall, for areas with high building density and high buildings, both the FAD of the buildings and the divisional density were high, which obstructed ventilation and resulted in relatively higher temperatures. Compared with summer, winter and fall vegetation have low impact on land surface temperature; buildings are one of the important driving factors for increasing land surface temperature, and high density and high-rise buildings are the strongest barrier to ventilation. Therefore, the FAD of a building has a correlation with surface temperature (0.44 and 0.42 in Fig. 9a and b, respectively). Spring and summer are plant growth seasons, and the number of leaves on the wood is high. Owing to the influence of building materials and other covers, the correlation between the FAD of the building and the surface temperature is weakened. For the LCZ5 type, the windward surface density of the buildings had the highest correlation with surface temperatures.

4. Discussion

4.1. Local climate zone wind environment in urban planning

Cities are open, complex, dynamic systems with global influence (Bai et al., 2018). The traditional approach to studying the sustainable development of urban ecosystems only considers a single factor of

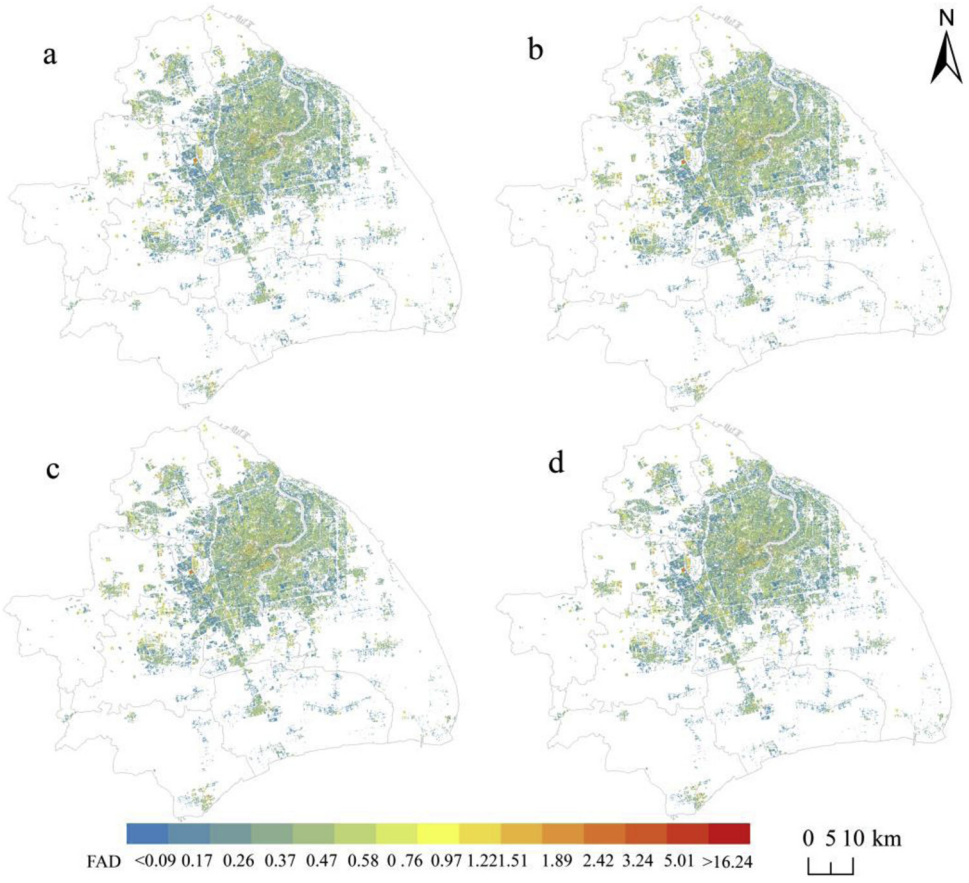

Fig. 7. Frontal area density (FAD) across Shanghai for the winter (a), spring (b), summer (c), and fall (d).

Table 4
Urban windward surface density (frontal area density; FAD) for Shanghai districts in 2017.

District	Area/km^2	Winter FAD	Spring FAD	Summer FAD	Fall FAD
Jingan	7.68	0.44–8.61	0.44–9.28	0.44–9.04	0.44–8.55
Putuo	55.43	0.04–5.18	0.04–5.52	0.04–5.45	0.04–5.17
Hongkou	23.53	0.07–10.76	0.07–11.48	0.07–11.31	0.07–10.69
Zhabei	29.32	0.08–6.37	0.08–6.72	0.08–6.74	0.08–6.42
Changning	36.96	0.04–6.02	0.04–6.28	0.04–6.22	0.04–5.95
Xuhui	54.81	0.11–6.87	0.11–7.37	0.11–7.22	0.11–6.82
Huangpu	20.43	0.10–6.93	0.10–7.44	0.10–7.38	0.10–6.98
Baoshan	294.32	0.15–4.23	0.15–4.39	0.15–4.45	0.15–4.26
Jiading	442.06	0.13–6.33	0.13–6.73	0.13–6.63	0.13–6.29
Qingpu	656.65	0.02–5.98	0.02–6.39	0.02–6.32	0.02–5.99
Jinshan	597.27	0.02–3.83	0.02–3.97	0.02–3.99	0.02–3.82
Yangpu	60.46	0.01–6.33	0.01–6.65	0.01–6.64	0.01–6.39
Songjiang	604.95	0.09–3.66	0.09–3.93	0.09–3.84	0.09–3.83
Pudong	1210.12	0.01–5.11	0.01–5.32	0.01–5.30	0.01–5.00
Minhang	373.39	0.13–3.62	0.13–3.88	0.13–3.81	0.13–3.60

ecological service values (Yang, Guan, Xia, Jin, & Li, 2018, Yang, Su et al., 2018), urban green infrastructure (Pelorosso, Gobattoni, & Leone, 2017), building configuration (Lan & Zhan, 2017), and non-urbanized spatial layout patterns (La Rosa & Privitera, 2013). The landscape combinations of cities of different scales are the key factor determining sustainable development (Azhdari, Soltani, & Alidadi, 2018; He, Zhao, Zhu, Darko, & Gou, 2018). The effective expression of urban morphological parameterization can show changes in climate performance within the city (Salvati, Palme, & de la Barrera, 2018), and climate change has an impact on the energy demand of the built environment (Chiesaa & Palmeb, 2018). Therefore, this study examined the impact of urban architectural spatial patterns on the thermal environment in local climate zones under natural wind conditions. By assessing the correlation between urban FAD and surface temperature without local climatic zones, the impact of buildings on urban climate under natural ventilation conditions was revealed. To achieve sustainable urban development, urban construction planning of new programs is needed to provide reference for future urban planning.

- Different local climatic zones provide climatic conditions corresponding to the urban environment (Verdonck et al., 2018). For megacities, the height and spacing of buildings are the main factors affecting urban climate (Cai, Ren, Xu, Lau, & Wang, 2017; Mou, He, Zhao, & Chau, 2017; Yang, Guan et al., 2018; Yang, Su et al., 2018). In vertical space, high-rise buildings generate heat by obstructing ventilation. In horizontal space, heat from the street is trapped by high-density buildings in horizontal space and is stored by building materials, so the surface temperature is increased. Owing to the differences in urban building categories, building performance heat consumption has a significant impact on the urban heat island effect, and thus affects the urban climate (Palme, Inostroza, Villacreses, Lobato-Cordero, & Carrasco, 2017; Palme, Inostroza, & Salvati, 2018). In assessing urban climate change and incorporating performance-based approaches, urban architectural patterns are one of the important drivers of climate change. As shown in Fig. 5, the city center mainly includes LCZ4, LCZ7, and LCZ8 types with high surface temperatures. High-density high-rise buildings can increase surface temperatures. With the rapid development of urbanization and the challenges of sustainable urban development (Geneletti, La Rosa, Spyra, & Cortinovis, 2017), the local climate types in areas surrounding the city are LCZ9 and LCZ10.
- Owing to seasonal differences in urban heat island effects (Peng, Jia,

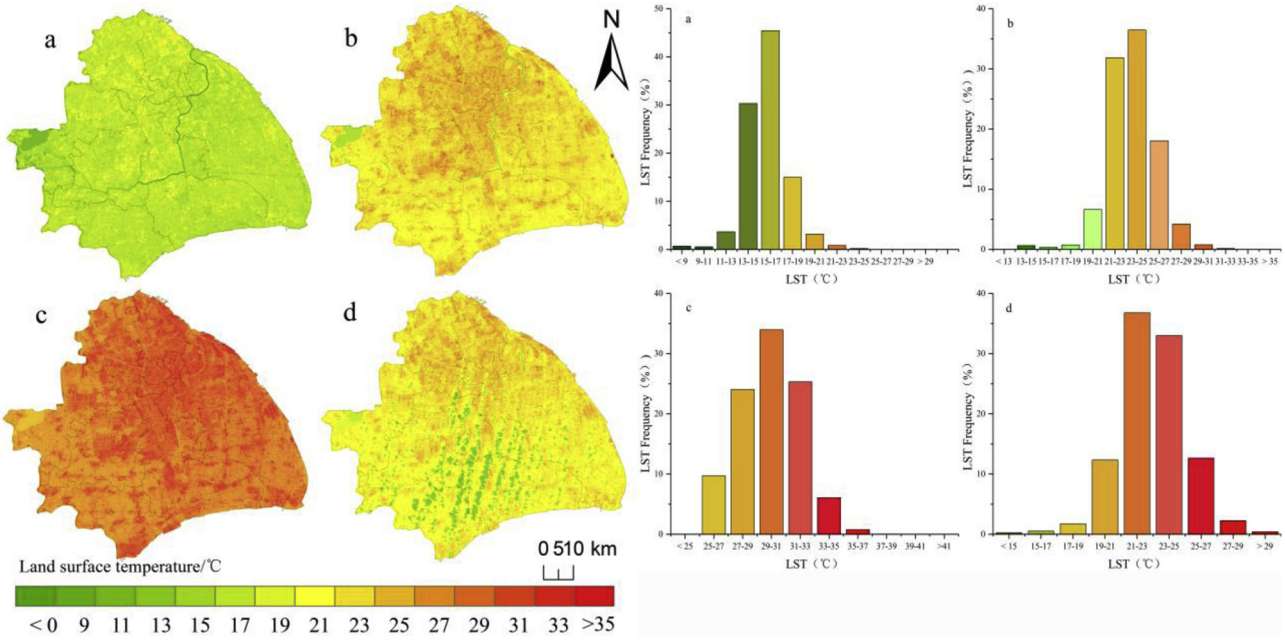

Fig. 8. Temperature distribution in Shanghai for the winter (a), spring (b), summer (c), and fall (d).

Liu, Li, & Wu, 2018; Zhou, Zhao et al., 2014; Zhou, Cadenasso et al., 2014), this study calculated the FAD and LST for four seasons of the year to reduce the impact of the underlying surface and provide better representation of actual climatic conditions. The difference in positive density was analyzed based on time and space. The results show that seasonal differences affected by wind direction are small. However, the same wind has different effects on the surface of urban buildings in different climate zones. The size of the wind frequency

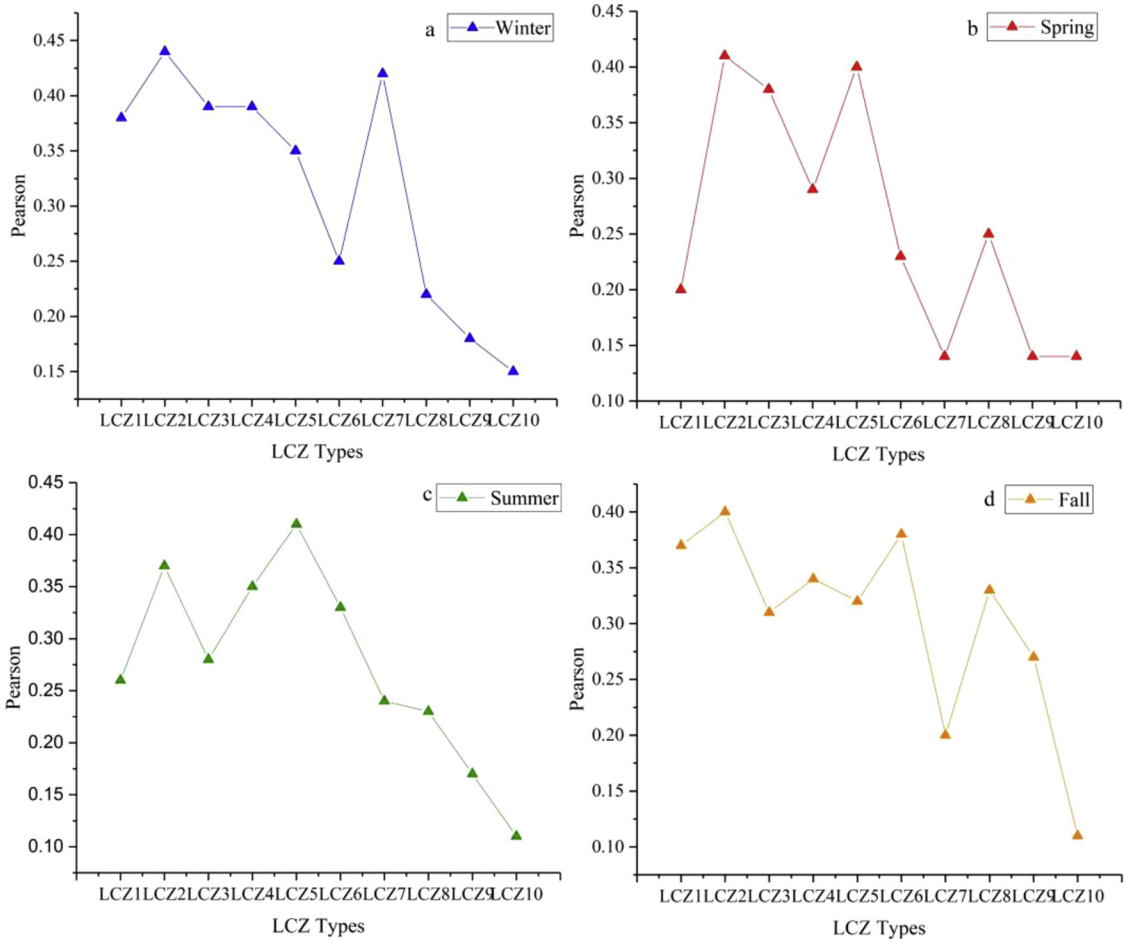

Fig. 9. Pearson's correlations between land surface temperature and frontal area density in the different local climate zones (LCZs) of different buildings.

is expressed as the intensity of the ventilation conditions, and the windward surface density indicates the interaction between the building and the wind environment. In this study, the quantitative parameter for performance-based planning was the FAD, indicating that the wind environment has an impact on surface temperature change. Good ventilation can improve the urban thermal environment effect. In the urban center, building height, building density, and the windward surface density are high, allowing the formation of dead zones for wind tunnels, and so the surface temperature increases; in urban fringe areas, building heights and building density are lower; the wind passes smoothly along wind channels, and as the land cover is mostly vegetation, the windward surface density is significantly reduced. As a result, the surface temperature is relatively low. Under the influence of natural wind conditions, the windward surface density method can be used to evaluate the obstruction effect of buildings on the wind; neatly arranged, open, and low-rise buildings allow winds to flow smoothly. The main prevailing wind direction in Shanghai is east, and so it is necessary to rely on a scientific wind direction layout when constructing urban ventilation corridors.

- In the four quarters, the frontal densities of buildings were positively correlated with the local surface temperature. In winter and spring, the highest coefficients of LCZ2 were 0.44 and 0.41, respectively; in summer, the highest coefficient (0.41) was found in LCZ5; in fall, the highest coefficient (0.40) was found in LCZ2. As a megacity, Shanghai has a complex urban morphology. LCZ2 and LCZ5 are distributed in various parts of the city, but are concentrated in the center. Therefore, the FAD contributes more to the LST. LCZ10 is more concentrated in the Qingpu and Songjiang districts of the urban fringe area, and the FAD is relatively small. Since urban surface temperature is also affected by other factors, including surface radiation, altitude, altitude, topographical morphology, general climatic conditions, and vegetation, the contribution of a single element to surface temperature is limited. For planners, reasonably arranged building space layout promotes effective ventilation along the ecological corridor, which is beneficial to the urban environment.
- **Implication for performance-based planning**: 1) the results of the different local climate zones defined by this study may be beneficial to be added to existing performance standards, which can be used for regulating local land use and protecting local communities from adverse impact of heat island. For example, regulation should be in place for LCZ4, LCZ7, and LCZ8 with high surface temperatures in the city areas to limit further high-rise building development in the areas and to incorporate heat island reduction strategies, such as green or cool roofs, cool pavements, or increased vegetation and trees. 2) Also this study measured frontal area density (FAD) and land surface temperature, these two indicators can contribute to the performance measure and zoning of the local areas by setting up a maximum local surface temperature limit, a maximum density limit and a maximum height limit for different local climate zones. 3) We measured the spatial distribution of FAD and LST for different local climate zones, which can be used to learn the optimal spatial composition of various buildings for heat prevention of local areas. It can also be incorporated into performance standards for the future design of desired climate performances of local urban zones.

4.2. Limitations

The results of this study reflect the thermal environmental effects of urban ecosystems from multiple perspectives such as building morphology and the local wind environment. To a certain extent, they will help planners to better establish urban ecosystems. However, the data are limited; we classified the local climate of the city and therefore focused more on buildings. The building data only contain building outlines and building heights, with building height calculated using floors, which may deviate from the actual building height. The impact of buildings with different functional types on the internal urban environment will be further explored in future research. Landsat 8 remote sensing is impacted by cloud cover. Therefore, only remote sensing images with less than 5% cloud cover were selected. The correlation method was selected to effectively analyze the relationship between urban FAD and local surface temperature, but spatial autocorrelation was not considered. Factors affecting urban climate are complex, and include topography, vegetation, and potential anthropogenic heat sources; these factors should be considered in future research.

5. Conclusions

To study the urban thermal environment effect, it is necessary to give priority to locality and determine the distribution characteristics of local buildings and surface temperature. The correlation between local climate zones' ventilation and surface temperatures were analyzed at a micro-scale. Taking urban architectural form as one of the characteristic factors for evaluating the applicability of land use, and using local temperature as the standard for evaluating urban performance, this research provides valuable information for assessing the urban heat island effect at this scale, and provides a reference for future urban planning. The results reveal a fair diversity of urban local climate zones; major types in the central urban area are LCZ4, LCZ7, and LCZ8, and those in the suburbs are LCZ5 and LCZ7. Therefore, in urban planning, considering the energy consumption of buildings, it is necessary to rationally arrange the spatial distribution of buildings to avoid the enhancement of the urban heat island effect.

The urban FAD shows little seasonal variation, and mainly depends on wind direction, wind frequency, and building surface shape. Remote sensing technology was used to obtain urban surface temperatures, and the distributions of buildings and urban surface temperatures show spatial homogeneity. Average surface temperatures for the winter, spring, summer, and fall were 15 °C, 23 °C, 30 °C, and 23 °C, respectively. The urban FAD is positively correlated with surface temperature. In spring, fall, and winter, the LCZ2 type sees the highest correlation between urban building area density and surface temperature. In the LCZ5 type in summer, the urban building area density has the highest correlation with surface temperature. Urban ventilation can reduce temperature, but it depends on the building surface area of the city. When planning a city, ventilation corridors should be constructed according to the distribution of the building space, so that buildings are arranged neatly and tightly.

Acknowledgments

This research study was supported by the National Natural Science Foundation of China (grant no. 41771178, 41630749, 41471140), Innovative Talents Support Program of Liaoning Province (Grant No. LR2017017) and the Liaoning Province Outstanding Youth Program (grant no. LJQ2015058). The authors would like to acknowledge all experts' contributions in the building of the model and the formulation of the strategies in this study.

References

Abd Razak, A., Hagishima, A., Ikegaya, N., & Tanimoto, J. (2013). Analysis of airflow over building arrays for assessment of urban wind environment. *Building and Environment, 59*, 56–65.

Azhdari, A., Soltani, A., & Alidadi, M. (2018). Urban morphology and landscape structure effect on land surface temperature: Evidence from Shiraz, a semi-arid city. *Sustainable Cities and Society, 41*, 853–864.

Bai, X. (2018). Advance the ecosystem approach in cities. *Nature, 559* 7-7.

Bai, X., Dawson, R. J., Ürge-Vorsatz, D., Delgado, G. C., Salisu Barau, A., Dhakal, S., et al. (2018). Six research priorities for cities and climate change. *Nature, 555*, 23–25.

Bai, X., McPhearson, T., Cleugh, H., Nagendra, H., Tong, X., Zhu, T., et al. (2017). Urbanization and the environment: Conceptual and empirical advances. *Annual Review of Environment and Resources, 42*, 215–240.

Baker, D. C., Sipe, N. G., & Gleeson, B. J. (2006). Performance-based planning: Perspectives from the United States, Australia, and New Zealand. *Journal of Planning Education and Research, 25*, 396–409.
Bernard, J., Musy, M., Calmet, I., Bocher, E., & Keravec, P. (2017). Urban heat island temporal and spatial variations: Empirical modeling from geographical and meteorological data. *Building and Environment, 125*, 423–438.
Bokaie, M., Zarkesh, M. K., Arasteh, P. D., & Hosseini, A. (2016). Assessment of Urban Heat Island based on the relationship between land surface temperature and Land Use/ Land Cover in Tehran. *Sustainable Cities and Society, 23*, 94–104.
Bottema, M., & Mestayer, P. G. (1998). Urban roughness mapping – Validation techniques and some first results. *Journal of Wind Engineering & Industrial Aerodynamics, 74–76*, 163–173.
Cai, M., Ren, C., Xu, Y., Lau, K. K., & Wang, R. (2017). Investigating the relationship between local climate zone and land surface temperature using an improved WUDAPT methodology – A case study of Yangtze River Delta, China. *Urban Climate,* 1–18.
Cao, C., Lee, X., Liu, S., Schultz, N., Xiao, W., Zhang, M., et al. (2016). Urban heat islands in China enhanced by haze pollution. *Nature Communications, 7*, 12509.
Chang, H., Xiang, C., Duan, C., Wan, Z., Liu, Y., Zheng, Y., et al. (2016). Study on the thermal performance and wind environment in a residential community. *International Journal of Hydrogen Energy, 41*, 15868–15878.
Chen, X., & Zhang, Y. (2017). Impacts of urban surface characteristics on spatiotemporal pattern of land surface temperature in Kunming of China. *Sustainable Cities and Society, 32*, 87–99.
Chiesaa, G., & Palmeb, M. (2018). Assessing climate change and urban heat island vulnerabilities in a built environment. *TECHNE-Journal of Technology for Architecture and Environment, 15*, 237–245.
China MOCP (2005). *Code for design of civil buildings. GB 50352-2005.* China Architecture & Building Press.
Dwivedi, A., & Khire, M. V. (2018). Application of split- window algorithm to study Urban Heat Island effect in Mumbai through land surface temperature approach. *Sustainable Cities and Society, 41*, 865–877.
Frew, T., Baker, D., & Donehue, P. (2016). Performance based planning in Queensland: A case of unintended plan-making outcomes. *Land Use Policy, 50*, 239–251.
Geneletti, D., La Rosa, D., Spyra, M., & Cortinovis, C. (2017). A review of approaches and challenges for sustainable planning in urban peripheries. *Landscape and Urban Planning, 165*, 231–243.
He, B., Yang, L., & Ye, M. (2014). Strategies for creating good wind environment around Chinese residences. *Sustainable Cities and Society, 10*, 174–183.
He, B., Zhao, D., Zhu, J., Darko, A., & Gou, Z. (2018). *Promoting and implementing urban sustainability in China: An integration of sustainable initiatives at different urban scales.* Habitat International.
Hsieh, C., & Huang, H. (2016). Mitigating urban heat islands: A method to identify potential wind corridor for cooling and ventilation. *Computers, Environment and Urban Systems, 57*, 130–143.
La Rosa, D., & Privitera, R. (2013). Characterization of non-urbanized areas for land-use planning of agricultural and green infrastructure in urban contexts. *Landscape and Urban Planning, 109*, 94–106.
Lan, Y., & Zhan, Q. (2017). How do urban buildings impact summer air temperature? The effects of building configurations in space and time. *Building and Environment, 125*, 88–98.
Liu, J., Cheng, H., Jiang, D., & Huang, L. (2019). Impact of climate-related changes to the timing of autumn foliage colouration on tourism in Japan. *Tourism Management, 70*, 262–272.
Liu, Y., Yue, W., Fan, P., Zhang, Z., & Huang, J. (2017). Assessing the urban environmental quality of mountainous cities: A case study in Chongqing, China. *Ecological Indicators, 81*, 132–145.
Liu, J., Wang, J., Wang, S., Wang, J., & Deng, G. (2018). Analysis and simulation of the spatiotemporal evolution pattern of tourism lands at the Natural World Heritage Site Jiuzhaigou, China. *Habitat International, 79*, 74–88.
Long, H., Liu, Y., Hou, X., Li, T., & Li, Y. (2014). Effects of land use transitions due to rapid urbanization on ecosystem services: Implications for urban planning in the new developing area of China. *Habitat International, 44*, 536–544.
Marwedel, J., & Marwedel, J. (1998). Opting for performance: An alternative to conventional zoning for land use regulation. *Journal of Planning Literature, 13*, 220–231.
Meng, F., He, B., Zhu, J., Zhao, D., Darko, A., & Zhao, Z. (2018). Sensitivity analysis of wind pressure coefficients on CAARC standard tall buildings in CFD simulations. *Journal of Building Engineering, 16*, 146–158.
Mou, B., He, B., Zhao, D., & Chau, K. (2017). Numerical simulation of the effects of building dimensional variation on wind pressure distribution. *Engineering Applications of Computational Fluid Mechanics, 11*, 293.
Nassar, A. K., Blackburn, G. A., & Whyatt, J. D. (2016). Dynamics and controls of urban heat sink and island phenomena in a desert city: Development of a local climate zone scheme using remotely-sensed inputs. *International Journal of Applied Earth Observation and Geoinformation, 51*, 76–90.
Ng, E., Yuan, C., Chen, L., Ren, C., & Fung, J. C. H. (2011). Improving the wind environment in high-density cities by understanding urban morphology and surface roughness: A study in Hong Kong. *Landscape and Urban Planning, 101*, 59–74.
O'Harrow, D. (1958). *Performance standards in industrial zoning: National Industrial Zoning Committee*.
Oke, T. R. (2006). Initial guidance to obtain representative meteorological observations at urban sites. *Geog.ubc.ca, 81*, 1–47.
Oke, T. R., Mills, G., Christen, A., & Voogt, J. A. (2017). *Urban climates.* Cambridge university press.
Ottensmann, J. R. (2005). Planning through the exchange of rights under performance zoning. *Economic Affairs, 25*, 40–43.
Palme, M., Inostroza, L., & Salvati, A. (2018). Technomass and cooling demand in South America: a superlinear relationship? *Building Research & Information, 46*, 864–880.
Palme, M., Inostroza, L., Villacreses, G., Lobato-Cordero, A., & Carrasco, C. (2017). From urban climate to energy consumption. Enhancing building performance simulation by including the urban heat island effect. *Energy and Buildings, 145*, 107–120.
Pelorosso, R., Gobattoni, F., & Leone, A. (2017). The low-entropy city: A thermodynamic approach to reconnect urban systems with nature. *Landscape and Urban Planning, 168*, 22–30.
Peng, F., Wong, M. S., Nichol, J. E., & Chan, P. W. (2016). Historical GIS data and changes in urban morphological parameters for the analysis of urban heat islands in Hong Kong. *ISPRS – International Archives of the Photogrammetry, Remote Sensing and Spatial Information Sciences, XLI-B2*, 55–62.
Peng, J., Jia, J., Liu, Y., Li, H., & Wu, J. (2018). Seasonal contrast of the dominant factors for spatial distribution of land surface temperature in urban areas. *Remote Sensing of Environment, 215*, 255–267.
Qiao, Z., Tian, G., & Xiao, L. (2013). Diurnal and seasonal impacts of urbanization on the urban thermal environment: A case study of Beijing using MODIS data. *ISPRS Journal of Photogrammetry and Remote Sensing, 85*, 93–101.
Qiao, Z., Xu, X., Wu, F., Luo, W., Wang, F., Liu, L., et al. (2017). Urban ventilation network model: A case study of the core zone of capital function in Beijing metropolitan area. *Journal of Cleaner Production, 168*, 526–535.
Qin, Z. H., Zhang, M. H., & Karnieli Berliner, A. P. (2001). Mono-window algorithm for retrieving land surface temperature from Landsat TM6 data. *Acta Geographica Sinica, 56*, 456–466.
Ribeiro, F. N. D., Oliveira, A. P. D., Soares, J., Miranda, R. M. D., Barlage, M., & Chen, F. (2018). Effect of sea breeze propagation on the urban boundary layer of the metropolitan region of Sao Paulo, Brazil. *Atmospheric Research, 214*, 174–188.
Rotem-Mindali, O., Michael, Y., Helman, D., & Lensky, I. M. (2015). The role of local land-use on the urban heat island effect of Tel Aviv as assessed from satellite remote sensing. *Applied Geography, 56*, 145–153.
Salvati, A., Palme, M., & de la Barrera, F. (2018). Urban morphology parameterization for climate modelling in urban planning. *International Conference on Urban Climate,* 4.
Santamouris, M., Cartalis, C., & Synnefa, A. (2015). Local urban warming, possible impacts and a resilience plan to climate change for the historical center of Athens, Greece. *Sustainable Cities and Society, 19*, 281–291.
Shen, L., Sun, J., & Yuan, R. (2018). Idealized large-eddy simulation study of interaction between urban heat island and sea breeze circulations. *Atmospheric Research, 214*, 338–347.
Shi, Y., Katzschner, L., & Ng, E. (2017). Modelling the fine-scale spatiotemporal pattern of urban heat island effect using land use regression approach in a megacity. *The Science of the Total Environment, 618*, 891–904.
Stewart, I. D., & Oke, T. R. (2012). Local climate zones for urban temperature studies. *Bulletin of the American Meteorological Society, 12*, 1879–1900.
Stewart, I. D., Oke, T. R., & Krayenhoff, E. S. (2014). Evaluation of the 'local climate zone' scheme using temperature observations and model simulations. *International Journal of Climatology, 34*, 1062–1080.
Verdonck, M., Demuzere, M., Hooyberghs, H., Beck, C., Cyrys, J., Schneider, A., et al. (2018). The potential of local climate zones maps as a heat stress assessment tool, supported by simulated air temperature data. *Landscape and Urban Planning, 178*, 183–197.
Voogt, J. A., & Oke, T. R. (2003). Thermal remote sensing of urban climates. *Remote Sensing of Environment, 86*, 370–384.
Wong, M. S., & Nichol, J. E. (2013). Spatial variability of frontal area index and its relationship with urban heat island intensity. *International Journal of Remote Sensing, 03*, 885–896.
Xu, Y., Ren, C., Ma, P., Ho, J., Wang, W., Lau, K. K., et al. (2017). Urban morphology detection and computation for urban climate research. *Landscape and Urban Planning, 167*, 212–224.
Yang, J., Sun, J., Ge, Q., & Li, X. (2017). Assessing the impacts of urbanization-associated green space on urban land surface temperature: A case study of Dalian, China. *Urban Forestry & Urban Greening,* 1–10.
Yang, J., Guan, Y., Xia, J. C., Jin, C., & Li, X. (2018). Spatiotemporal variation characteristics of green space ecosystem service value at urban fringes: A case study on Ganjingzi District in Dalian, China. *The Science of the Total Environment, 639*, 1453–1461.
Yang, J., Su, J., Xia, J. C., Jin, C., Li, X., & Ge, Q. (2018). The impact of spatial form of urban architecture on the urban thermal environment: A case study of the Zhongshan District, Dalian, China. *IEEE Journal of Selected Topics in Applied Earth Observations & Remote Sensing, 11*, 2709–2716.
Yin, C., Yuan, M., Lu, Y., Huang, Y., & Liu, Y. (2018). Effects of urban form on the urban heat island effect based on spatial regression model. *The Science of the Total Environment, 634*, 696–704.
Yuan, C., Ren, C., & Ng, E. (2014). GIS-based surface roughness evaluation in the urban planning system to improve the wind environment – A study in Wuhan, China. *Urban Climate, 10*, 585–593.
Yue, W., Liu, Y., & Fan, P. (2013). Measuring urban sprawl and its drivers in large Chinese cities: The case of Hangzhou. *Land Use Policy, 31*, 358–370.
Zhang, Y., & Gu, Z. (2013). Air quality by urban design. *Nature Geoscience, 6*, 506.
Zhao, D., He, B., & Meng, F. (2015). The green school project: A means of speeding up sustainable development? *Geoforum, 65*, 310–313.
Zheng, Y., Ren, C., Xu, Y., Wang, R., Ho, J., Lau, K., et al. (2017). GIS-based mapping of local climate zone in the high-density city of Hong Kong. *Urban Climate,* 1–30.
Zhou, W., Huang, G., & Cadenasso, M. L. (2011). Does spatial configuration matter? Understanding the effects of land cover pattern on land surface temperature in urban landscapes. *Landscape and Urban Planning, 102*, 54–63.
Zhou, Y., Weng, Q., Gurney, K. R., Shuai, Y., & Hu, X. (2012). Estimation of the

relationship between remotely sensed anthropogenic heat discharge and building energy use. *ISPRS Journal of Photogrammetry and Remote Sensing, 67*, 65–72.
Zhou, W., Cadenasso, M., Schwarz, K., & Pickett, S. (2014). Quantifying spatial heterogeneity in urban landscapes: Integrating visual interpretation and object-based classification. *Remote Sensing, 6*, 3369–3386.
Zhou, D., Zhao, S., Liu, S., Zhang, L., & Zhu, C. (2014). Surface urban heat island in China's 32 major cities: Spatial patterns and drivers. *Remote Sensing of Environment, 152*, 51–61.
Zhu, Z., Woodcock, C. E., Rogan, J., & Kellndorfer, J. (2012). Assessment of spectral, polarimetric, temporal, and spatial dimensions for urban and peri-urban land cover classification using Landsat and SAR data. *Remote Sensing of Environment, 117*, 72–82.